SUPPORTING INFORMATION

Photo-activated process cascaded electrocatalysis for highly efficient CO_2 reduction over core-shell ZIF-8@Co/C

Jian-Xia Gu, [a] Xue Zhao, [a] Yue Sun, [b] Jie Zhou, [a] Chun-Yi Sun, [a, *] Xin-Long Wang, [a, *] Zhen-Hui Kang, [b, *] Zhong-Min Su[a]

[a.] National & Local United Engineering Laboratory for Power Batteries

Department of Chemistry

Northeast Normal University

Changchun 130024, China

E-mail: suncy009@nenu.edu.cn; wangxl824@nenu.edu.cn.

[b.] Jiangsu Key Laboratory for Carbon-Based Functional Materials & Devices

Institute of Functional Nano & Soft Materials (FUNSOM)

Soochow University

Suzhou 215123, China

E-mail: zhkang@suda.edu.cn

[b.] Institute of Advanced Materials

Northeast Normal University

5268 Renmin Street, Changchun 130024, P.R. China.

E-mail: zhkang@suda.edu.cn

Table of Contents

Experimental details

Characterizations

The powder X-ray diffraction patterns (PXRD) were obtained on a SmartLab X-ray diffractometer through using a JEM-2100Plus. Transmission electron microscopy (TEM) and high-resolution TEM (HRTEM) images were acquired from a JEM-2010 transmission electron microscope at an accelerating voltage of 200 kV. The elemental mappings and line scans of samples were determined by EDX equipped on TEM. Inductively coupled plasma mass spectrometry (ICP-MS) was conducted on Agilent 7500a Inductively Coupled Plasma Mass Spectrometry (ICP-MS 7500). X-ray photoelectron spectroscopy (XPS) characterizations were performed on an Escalab 250 instrument. N_2 and CO_2 adsorption-desorption isotherms can be conducted on an ASAP 2020 Micromeritics (USA). The optical absorption behaviors of samples were studied by the UV-Vis spectrometer (U-3010 spectrophotometer, Hitachi, Japan). The gas products in electrocatalytic and light-irradiation cascaded electrocatalytic reaction were measured by Shimadzu Gas Chromatography (GC). The transient photovoltage (TPV) responses were carried out by a homemade measurement system.

Preparation of ZIF-8 Seeds[1]

$Zn(NO_3)_2{\cdot}6H_2O$ (810 mg) and 2-MeIm (526 mg) were dissolved in 40 mL of methanol, respectively. Then, the two kinds of solutions were mixed under stirring and reacted for 12 h at room temperature. Finally, the white powder was collected by centrifugation, washed five times with methanol, and dried in the vacuum oven at 80 °C overnight.

Preparation of ZIF-67[1]

519 mg of cobalt chloride ($CoCl_2.6H_2O$) and 600 mg of polyvinylpyrrolidone (PVP) were dissolved in 40 mL methanol, then a methanolic solutions (80 mL) of 2-MeIm (2630 mg) was mixed under stirring. The ZIF-67 was obtained after reacting for 12 h at room temperature. Last, the collection process of purple powder was similar to that of ZIF-8.

Optimization of the applied potentials for light-irradiation cascaded electrochemical reduction of CO_2

According to LSV (Fig. 4 and Figure S8), the applied potentials also significantly influenced the reactivity of the reduction of CO_2, so the potential was optimized by measuring the amount of products at different potentials from -0.7 V to -1.0 V vs. RHE on ZIF-8@Co/C-x (x=1 to 5, Figure S9). The production rates of CO and H_2 increase gradually when the external circuit potentials rise on each ZIF-8@Co/C-x catalyst. Until the external circuit voltage is at -1.0 V vs. RHE, the production rate of CO decrease lightly, which may be because the competition of generating H_2 becomes greater at high potential. Therefore, we chosen the -0.9 V vs. RHE as the best potential for follow-up research.

Energy Efficiency Calculation

Energy efficiency (EE) is critical parameter to evaluate overall energy utilization of reactions. In this work, energy efficiency was determined by the following Equation[2]:

$$\mathrm{EE}(\%) = \Delta E^{0} \,/\, \Delta E^{\mathrm{Applied}} \times \mathrm{FE}$$

where ΔE^0 is the equilibrium full cell potential, $\Delta E^{\mathrm{Applied}}$ is the applied full cell potential and FE is the average Faradaic efficiency for CO and H_2 at −0.9 V.

Results and Discussion

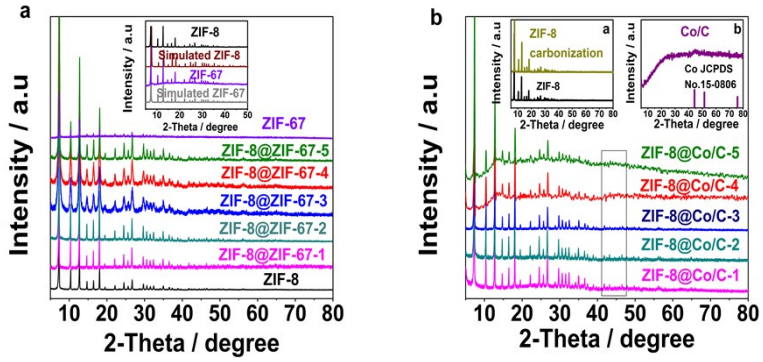

Figure S1. The PXRD of (a) ZIF-8, ZIF-67 and ZIF-8@ZIF-67-x, (b) ZIF-8 carbonization, Co/C (carbonization of ZIF-67) and ZIF-8@Co/C-x.

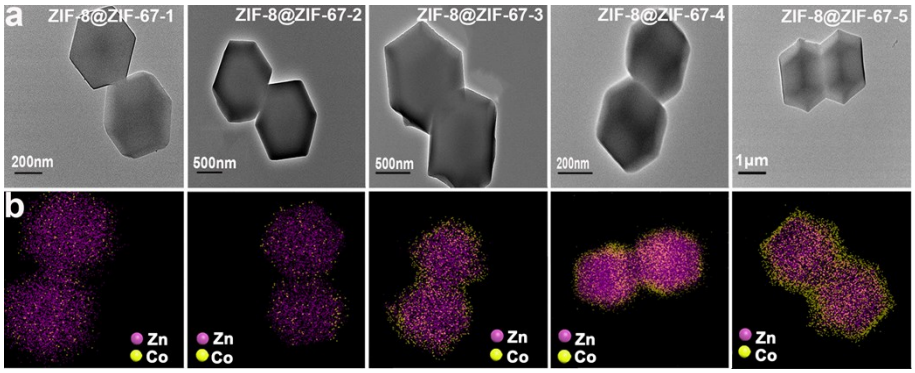

Figure S2. The (a) TEM images and (b) elemental mappings of ZIF-8@ZIF-67-x (x=1 to 5): Zn (purple) and Co (yellow).

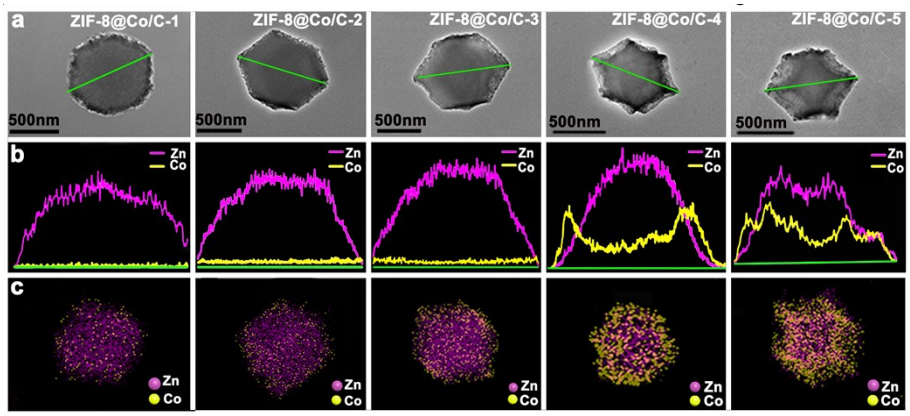

Figure S3. The (a) TEM images, (b) line-scanning spectra and (c) elemental mappings of ZIF-8@ZIF-67-x (x=1 to 5): Zn (purple) and Co (yellow).

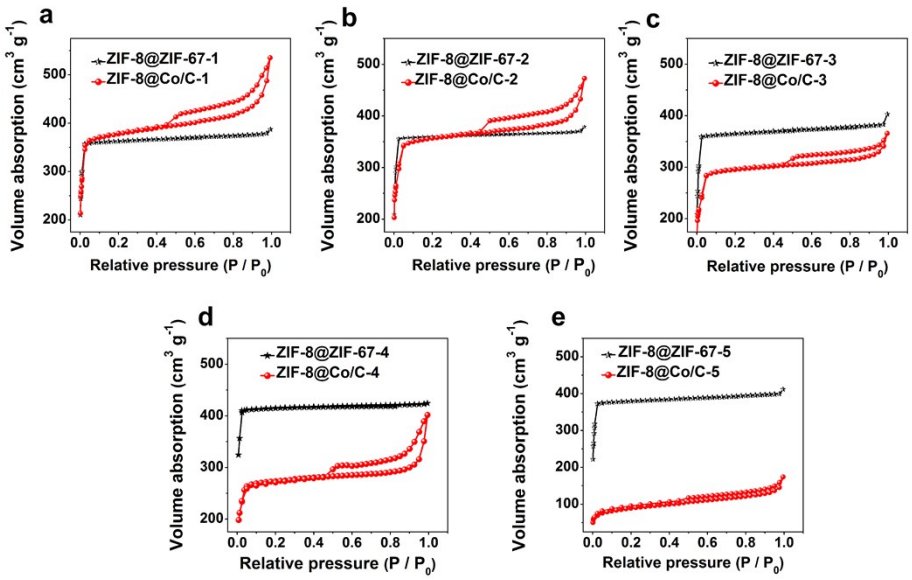

Figure S4 The N_2 adsorption-desorption curves of ZIF-8@ZIF-67-x and ZIF-8@Co/C-x (x=1-5).

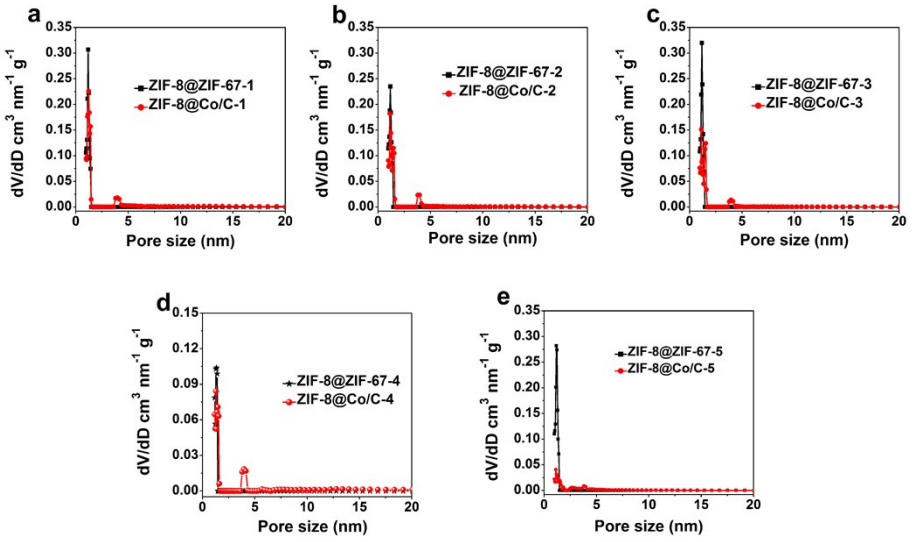

Figure S5 The pore size distribution of ZIF-8@ZIF-67-x and ZIF-8@Co/C-x (x=1-5).

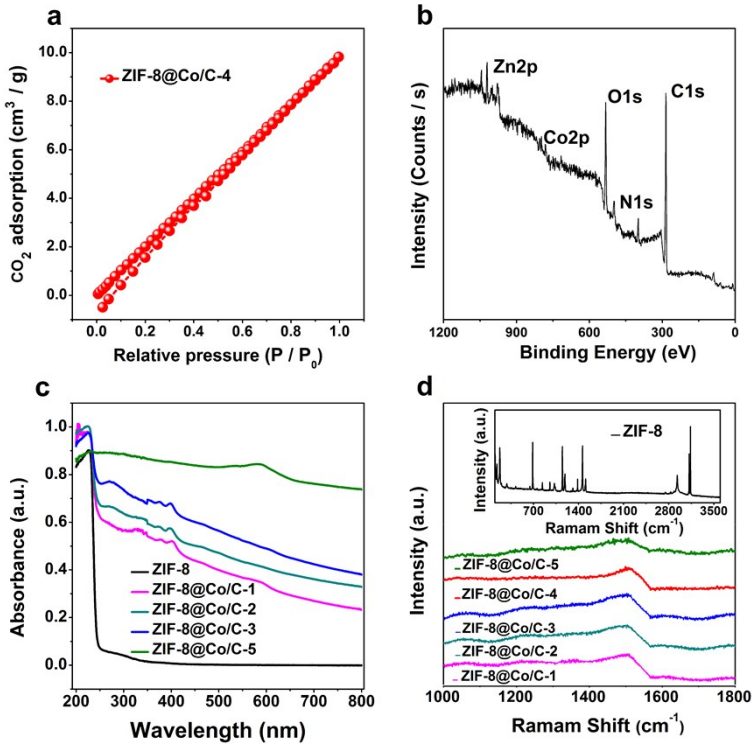

Figure S6. (a) CO_2 physisorption isotherms of ZIF-8@Co/C-4. (b) XPS survey spectrum of ZIF-8@Co/C-4. (c) UV-Vis spectra of ZIF-8 and ZIF-8@Co/C-x (x=1-5). (d) The Raman shift of ZIF-8 and ZIF-8@Co/C-x (x=1-5).

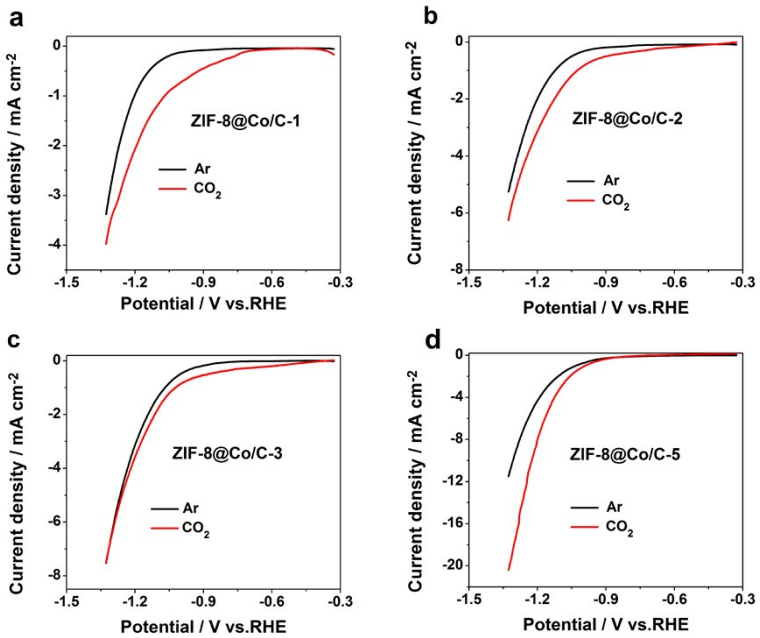

Figure S7. The LSV of ZIF-8@Co/C-x on GCE in the Ar- and CO_2-saturated K_2SO_4 solution.

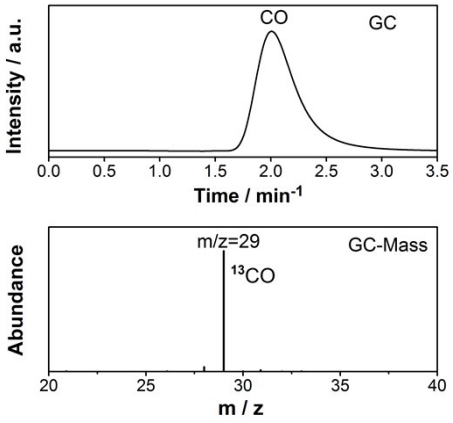

Figure S8. GC-MS result of isotopic experiment under $^{13}CO_2$ atmosphere.

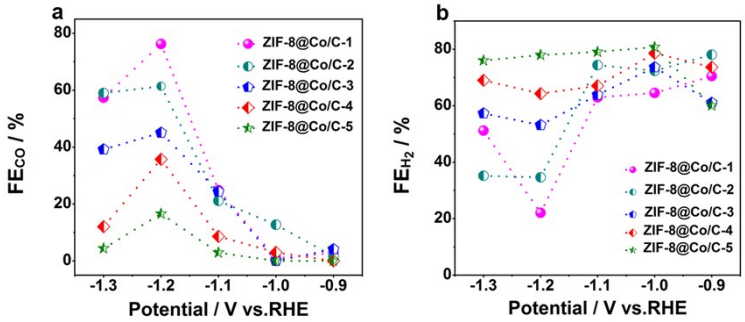

Figure S9. The Faradaic efficiency for CO (a) and H_2 (b) on the ZIF-8@Co/C-x at different applied potentials.

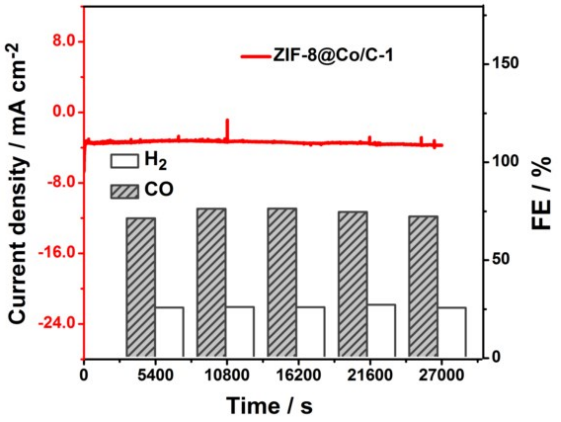

Figure. S10 The electrocatalytic stability of ZIF-8@Co/C-1 at an applied potential of -1.2 V vs. RHE in the CO_2-saturated K_2SO_4.

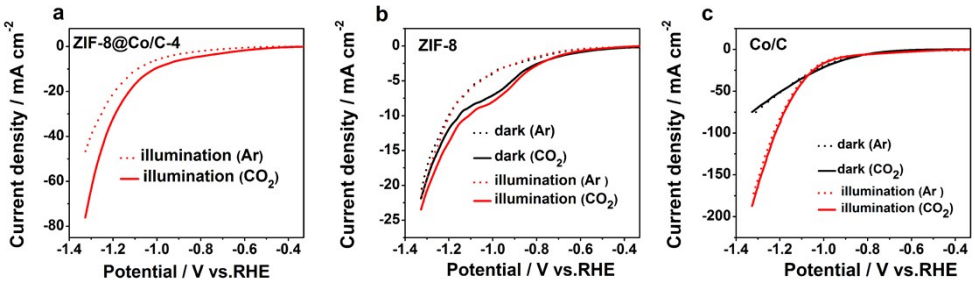

Figure S11. The LSV responses of ZIF-8@Co/C-4 (a), ZIF-8 (b) and Co/C (c) in 0.25 M Ar- and CO_2-saturated K_2SO_4 on carbon paper .

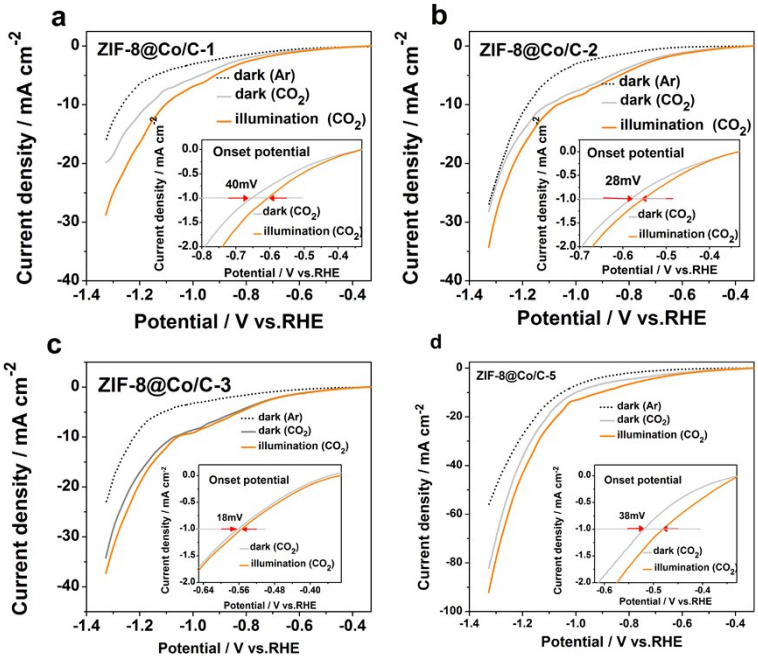

Figure S12. The LSV responses of ZIF-8@Co/C-x in Ar-saturated 0.25 M K_2SO_4 in the dark (black line) and CO_2-saturated 0.25 M K_2SO_4 under illumination (orange line) /dark (gray line).

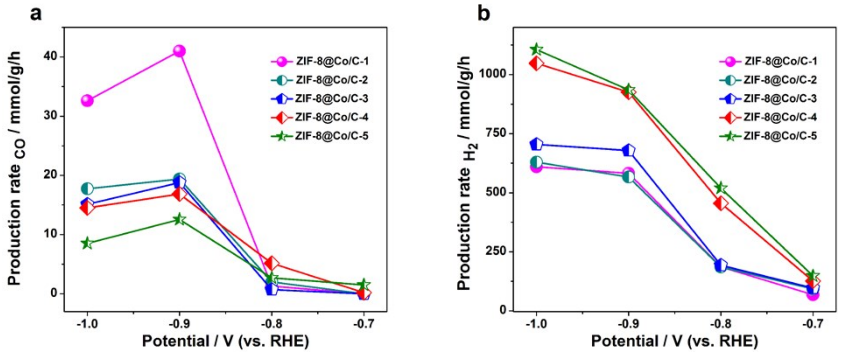

Figure S13. The production rates of (a) CO and (b) H_2 for ZIF-8@Co/C-x at different applied potentials by light irradiation.

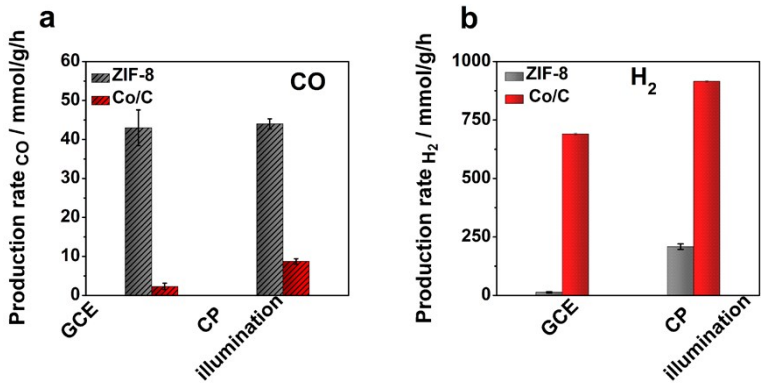

Figure S14. The production rates of (a) CO and (b) H_2 for ZIF-8 and Co/C on GCE and CP.

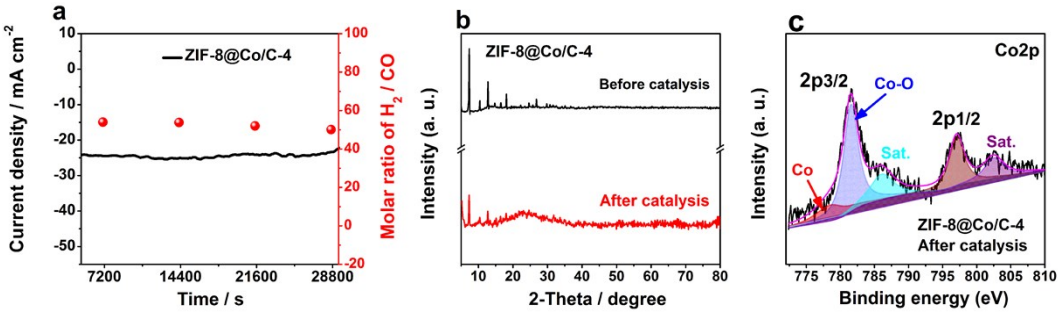

Figure S15. (a)The photostability of ZIF-8@Co/C-4 at an applied potential of -0.9 V vs. RHE in the CO_2-saturated K_2SO_4. (b) XRD pattern of ZIF-8@Co/C-4 after reaction for 8h. (c) XPS of Co2p after catalysis raection for 8h.

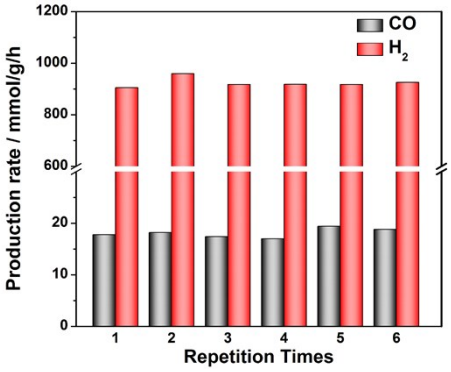

Figure S16 The reproducibility of ZIF-8@Co/C-4 towards electrochemical reduction of CO_2 under illumination.

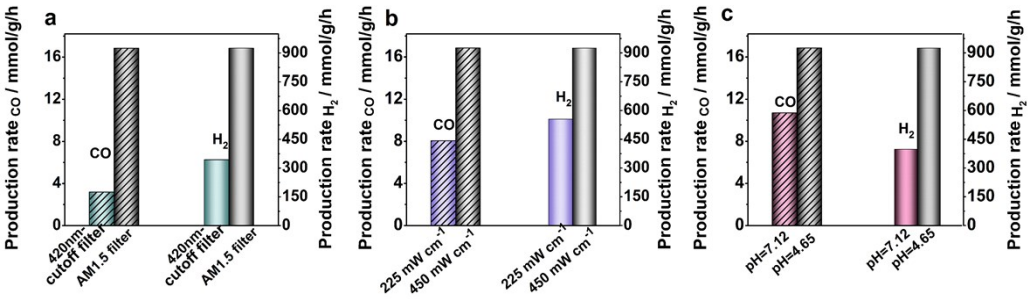

Figure S17. The effect of external factors including (a) optical wavelength, (b) light density and (c) pH of electrolyte solution on the light-irradiation cascaded electrocatalytic reduction of CO_2 to prepare syngas over ZIF-8@Co/C-4 catalyst.

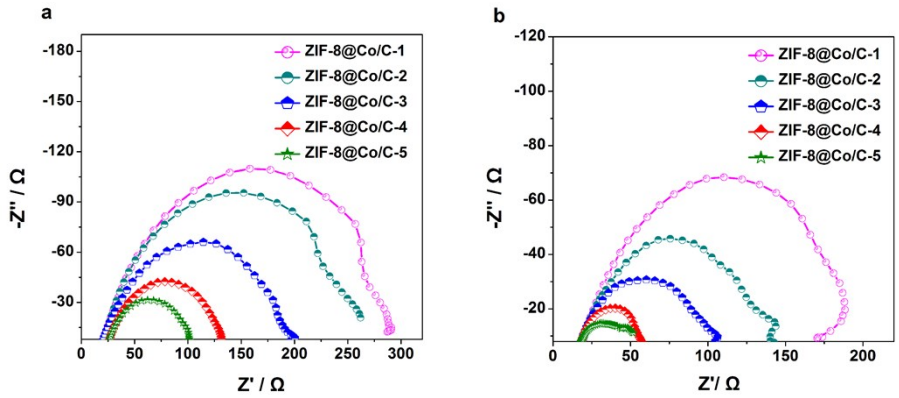

Figure S18. Electrochemical impedance spetra (EIS) of ZIF-8@Co/C-x in CO_2-saturated K_2SO_4 (0.25M) solution without illumination (a) and with illumination (b).

Table S1. The amount of $CoCl_2 \cdot 6H_2O$, 2-MeIm and in the synthetic process of ZIF-8@Co/C-x.

Sample Number	$CoCl_2 \cdot 6H_2O$ [mg]	2-MeIm [mg]	Methanol [mL]
ZIF-8@ZIF-67-1	8.9	44.8	0.15
ZIF-8@ZIF-67-2	11.1	55.9	0.19
ZIF-8@ZIF-67-3	17.7	89.5	0.3
ZIF-8@ZIF-67-4	177	895	3.0
ZIF-8@ZIF-67-5	354	1790	6.0

Table S2. Summary on the molar ratios of Co^{2+}/Zn^{2+} and the thicknesses of Co/C shell in core–shell ZIF-8@Co/C-x.

Sample Number	Molar ratio of Co^{2+}/Zn^{2+}	Shell thickness [nm]
ZIF-8@Co/C-1	0.04	10
ZIF-8@Co/C-2	0.08	14
ZIF-8@Co/C-3	0.31	20
ZIF-8@Co/C-4	0.56	50
ZIF-8@Co/C-5	0.78	111

Table S3 Comparison of specific surface area of ZIF-8@ZIF-67-x and ZIF-8@Co/C-x (x=1-5).

Samples	S_{BET} (m^2 g^{-1})	Samples	S_{BET} (m^2 g^{-1})	Percentage of change
ZIF-8@ZIF-67-1	1584	ZIF-8@Co/C-1	1567	1%
ZIF-8@ZIF-67-2	1581	ZIF-8@Co/C-2	1452	8%
ZIF-8@ZIF-67-3	1597	ZIF-8@Co/C-3	1197	30%
ZIF-8@ZIF-67-4	1538	ZIF-8@Co/C-4	851	40%
ZIF-8@ZIF-67-5	1657	ZIF-8@Co/C-5	325	80%

Table S4 The ratios of syngas (CO/H_2) on different catalysts in the electrochemical reduction of CO_2

Electrocatalysts	**Ratios of Syngas (CO/H_2)**	**Reference**
Hydrophobic exfoliated MoS_2 (H-E-MoS_2)	1:2 to 4:1	3
CdS_xSe_{1-x} nanorods	4:1 to 1:4	4
Ag NWs (35 nm) electrode	1:1 to 4:1	5
Co-HNC (ZnO@Zn/Co-ZIF)	1:2	6
core/shell Cu/In_2O_3 nanoparticles	2.5:1 to 1:4	7
MoSeS alloy monolayers	1:1	8
Zn-3 catalyst	0.2 to 2.31	9
Au NPs / TiNS	3:1 to1:3	10
ZIF-8@Co/C-x (x=1 to 5)	**3:1 to 1:5**	**This Work**

Table S5. The solar-to-syngas energy conversion efficiency (Joule-to-Joule) of ZIF-8@Co/C-x.

Catalyst	**Yield of syngas [μmol]**				**Conversion efficiency (Joule-to-Joule)**
	Dark		**Illumination**		
	CO	**H_2**	**CO**	**H_2**	
ZIF-8@Co/C-1	2.30	26.1	9.9	125.9	3.79%
ZIF-8@Co/C-2	1.5	24.1	3.7	109.7	3.23%
ZIF-8@Co/C-3	0.9	34.0	3.8	135.8	3.69%
ZIF-8@Co/C-4	1.1	35.0	3.4	185.1	5.38%
ZIF-8@Co/C-5	1.0	49.5	2.5	187.1	4.91%

Table S6 Solar-to-syngas energy conversion efficiency of reported systems.

Device	Electrode materials	Solar-to-syngas energy conversion efficiency	Reference
Photoelectrode-photovoltaic (PV) dual absorber tandem system	ZnO@ZnTe@CdTe-Au	0.43%	11
Three-electrode cell	Pt-TiO_2/GaN/n^+-p Si	0.87%	12
Filter-press reactor	Cu-Zn cathode: Silicon HIT cell with Ni foam photoanode	4.3%.	13
H-type PEC tandem cell	a-Si/TiO_2/7Au or a-Si/TiO_2/4Au photocathodes and $BiVO_4$/ FeOOH/NiOOH photoanodes	0.29% / 0.27%	14
Silicon photovoltaic cells with catalysts	β-FeOOH: Ni/a-Ni$(OH)_2$	3.4%	15
Three-electrode cell	Au/p-ZnTe	0.005%	16
PV-APS cell	Single-site Ni-SNG cathode: N-TiO2 nanorods array	5.15%	17
Photo-irradiation three-electrode cell	**ZIF-8@Co/C-4**	**5.38%**	**This work**

References

1 J. Tang, R. R. Salunkhe, J. Liu, N. L. Torad, M. Imura, S. Furukawa and Y. Yamauchi, *J. Am. Chem. Soc.*, 2015, **137**, 1572-1580.

2 J. Choi, P. Wagner, R. Jalili, J. Kim, D. R. MacFarlane, G. G. Wallace and D. L. Officer, *Adv. Energy Mater.*, 2018, **8**, 1801280.

3 K. Lv, C. Teng, M. Shi, Y. Yuan, Y. Zhu, J. Wang, Z. Kong, X. Lu and Y. Zhu, *Adv. Funct. Mater.*, 2018, **28**, 1802339.

4 R. He, A. Zhang, Y. Ding, T. Kong, Q. Xiao, H. Li, Y. Liu and J. Zeng, *Adv. Mater.*, 2018, **30**, 1705872.

5 W. Xi, R. Ma, H. Wang, Z. Gao, W. Zhang and Y. Zhao, *ACS Sustainable Chem. Eng.*, 2018, **6**, 7687-7694.

6 X. Song, H. Zhang, Y. Yang, B. Zhang, M. Zuo, X. Cao, J. Sun, C. Lin, X. Li and Z. Jiang, *Adv.Sci.*, 2018, **5**, 1800177.

7 H. Xie, S. Chen, F. Ma, J. Liang, Z. Miao, T. Wang, H.-L. Wang, Y. Huang and Q. Li, *ACS Appl. Mater. Interfaces.,* 2018, **10**, 36996-37004.

8 J. Xu, X. Li, W. Liu, Y. Sun, Z. Ju, T. Yao, C. Wang, H. Ju, J. Zhu, S. Wei and Y. Xie, *Angew. Chem. Int. Ed.,* 2017, **56**, 9121-9125.

9 B. Qin, Y. Li, H. Fu, H. Wang, S. Chen, Z. Liu and F. Peng, *ACS Appl. Mater. Interfaces.*, 2018, **10**, 20530-20539.

10 F. Marques Mota, D. L. T. Nguyen, J.-E. Lee, H. Piao, J.-H. Choy, Y. J. Hwang and D. H. Kim, *ACS Catal.,* 2018, **8**, 4364-4374.

11 Y. J. Jang, I. Jeong, J. Lee, J. Lee, M. J. Ko and J. S. Lee, *ACS Nano.*, 2016, **10**, 6980-6987.

12 S. Chu, P. Ou, P. Ghamari, S. Vanka, B. Zhou, I. Shih, J. Song and Z. Mi, *J. Am. Chem. Soc.,* 2018, **140**, 7869-7877.

13 F. Urbain, P. Tang, N. M. Carretero, T. Andreu, L. G. Gerling, C. Voz, J. Arbiol and J. R. Morante, *Energy Environ. Sci.*, 2017, **10**, 2256-2266.

14 C. Li, T. Wang, B. Liu, M. Chen, A. Li, G. Zhang, M. Du, H. Wang, S. F. Liu and J. Gong, *Energy Environ. Sci.*, 2019, **12**, 923-928.

15 T. Arai, S. Sato, K. Sekizawa, T. M. Suzuki and T. Morikawa, *Chem. Commun.*, 2019, **55**, 237-240.

16 Y. J. Jang, J.-W. Jang, J. Lee, J. H. Kim, H. Kumagai, J. Lee, T. Minegishi, J. Kubota, K. Domen and J. S. Lee, *Energy Environ. Sci.,* 2015, **8**, 3597-3604.

17 H. Zhang, J. Ming, J. Zhao, Q. Gu, C. Xu, Z. Ding, R. Yuan, Z. Zhang, H. Lin, X. Wang and J. Long, *Angew. Chem. Int. Ed.*, 2019, **58**, 7718-7722.